International Journal of Automotive Technology, Vol. 21, No. 4, pp. 903–917 (2020)
DOI 10.1007/s12239–020–0087–7

pISSN 1229–9138/ eISSN 1976–3832

COLLISION AVOIDANCE OF LOW SPEED AUTONOMOUS SHUTTLES WITH PEDESTRIANS

Sukru Yaren Gelbal[1, 2], Bilin Aksun-Guvenc[1, 3] and Levent Guvenc[1,2,3)*]

[1)]Automated Driving Lab, The Ohio State University, Columbus 43212, USA
[2)]Department of Electrical and Computer Engineering, The Ohio State University, Columbus 43210, USA
[3)]Department of Mechanical and Aerospace Engineering, The Ohio State University, Columbus 43210, USA

(Received 26 March 2019; Revised 17 August 2019; Accepted 5 November 2019)

ABSTRACT–This paper is on a pedestrian collision avoidance system for low speed autonomous shuttles based on Vehicle-to-Pedestrian (V2P) communication. When pedestrians cannot be detected using line-of-sight sensors like camera, radar and LIDAR, V2P communication with the Dedicated Short Range Communication (DSRC) enabled pedestrian smartphone is used to detect and localize them through the in-vehicle DSRC radio used for Vehicle-to-Everything (V2X) communication. The vehicle, then, either stops or, if possible, goes around the pedestrian in a socially acceptable manner using the elastic band method for locally modifying the vehicle trajectory in real time. The elastic band method of collision avoidance is modified for fast real time execution in this paper. Along with model-in-the-loop simulations, a hardware-in-the-loop simulator using an automated driving vehicle model in the high fidelity vehicle dynamics simulation program Carsim Real Time with Sensors and Traffic with two DSRC modems emulating the vehicle and pedestrian communications is introduced and used in this paper as a prerequisite to real world experiments. Both stationary and moving pedestrians are considered in the model and hardware-in-the-loop simulations. Two real world experiments are also presented to demonstrate the V2P based avoidance of crashes between low speed autonomous shuttles and pedestrians.

KEY WORDS : Pedestrian collision avoidance, Connected collision avoidance, Elastic band method

1. INTRODUCTION

Connected and autonomous vehicles (CAV) are expected to be available in series production in the near to mid-term future according to Guvenc *et al*. (2017b). Actively avoiding crashes is an important field of current research for both driver piloted and autonomous vehicles. The World Health Organization predicts that by 2020, road traffic injuries due to crashes will rise in total number by 65 % and will be the third highest cause of disability-adjusted life years. Cooperative safety systems based on vehicular communications can significantly decrease the number of road crashes (Paier *et al*., 2010). The U.S. Department of Transportation (DOT) has estimated that Vehicle-to-Vehicle (V2V) communication can address up to 82 % of all crashes in the United States involving unimpaired drivers, potentially saving thousands of lives (Kenney, 2011). Connected vehicles can talk to each other so that they can prevent traffic crashes and also enable safety, mobility and environmental benefits.

Pedestrians are among the most exposed road users in lethal collisions (Gandhi and Trivedi, 2007; WHO, 2011; Bagheri *et al*., 2016), and pedestrian safety is a priority for the U.S. Federal Highway Administration's Office of Safety (Swanson *et al*., 2016). The City of New York, for example, is exploring technology for improving pedestrian safety (Hickey, 2016). More than 4,000 pedestrians are killed in traffic accidents each year only in America according to the statistics of the National Highway Traffic Safety Administration (NHTSA). The U.S. Department of Transportation is, therefore, aggressively working towards the deployment of connected vehicle technologies that can prevent crashes involving pedestrians (United States Department of Transportation, 2017).

Safety critical applications of connected and autonomous vehicles are among the most significant intelligent transportation systems based on communication technologies. The detection range for perception sensors are on the order of tens of meters, but communication equipment's range is on the order of hundreds of meters (Cho, 2014). Another major drawback of autonomous vehicles that use perception sensors (radar, LIDAR, camera) (Gandhi and Trivedi, 2007) alone in obstacle detection is their dependence on line-of-sight which makes them unusable in Non-Line-of-Sight (NLOS) conditions. They have difficulty in seeing or sensing obstacles which are blocked by vehicles, trees or building corners and the other side of hilly/curved roads (Bagheri *et al*., 2016), as well as bad weather conditions, fog, snow. Although sensor fusion can challenge this to some extent, the NLOS

*Corresponding author. e-mail: guvenc.1@osu.edu

scenarios will not be fully resolved even then (Gandhi and Trivedi, 2007; David and Flac, 2010; Bagheri *et al*., 2016). Under these conditions, it is also difficult for drivers to notice the pedestrian in time and avoid the accident.

Under NLOS, vehicle-to-pedestrian communication can be used to exchange messages between road users, sending their information (location, speed, direction, etc.) (Bagheri *et al*., 2016). Different technologies (Wi-Fi, cellular technologies, DSRC) were used in V2X communication systems to alert collision risk with pedestrians in the literature (Ho and Chen, 2017). The approach in this paper is applicable for all of these different ways of implementing V2P communication. DSRC based V2P was used in the experiments here as these modems were available in our lab. Our collision avoidance based on V2P approach is general in nature and will also work with other forms of V2P communication like Wi-Fi or cellular communication.

Five priority pre-crash scenarios addressable by V2P-based crash avoidance technology were selected by U.S. DOT National Highway Traffic Safety Administration. These priority scenarios account for 79 % of all target pedestrian crashes and 91 percent of the deadly pedestrian crashes (Swanson *et al*., 2016). Therefore, in this paper we assume that all pedestrian smartphones are either equipped with V2P communication capability or are able to communicate with the road side unit in a nearby traffic light which will then broadcast this information using its DSRC modem.

Crash or collision avoidance is the most important objective of safety critical applications in connected vehicles (Wang *et al*., 2012; Jiménez *et al*., 2015; Verma *et al*., 2015). As a result, there are a lot of different collision avoidance algorithms that are available in the literature. In this paper, we concentrate on the elastic band method of collision avoidance which was first proposed by Quinlan and Khatib (1993) for mobile robots. This method was applied to road vehicle based applications for highway driving by Ararat and Aksun-Guvenc in Ararat and Aksun-Guvenc (2008). In a mixed traffic environment where there are also pedestrians, socially acceptable distance needs to be considered in order to respect the personal space of people. A modified elastic band method was, thus, developed in Emirler *et al*. (2016) to avoid collision with pedestrians at a socially acceptable distance. The elastic band method of (Ararat and Aksun-Guvenc, 2008; Emirler *et al*., 2016) will be used in this paper as it is easy to implement in real time for autonomous vehicles where the desired route is known or can be calculated.

The elastic band method is extended in this paper into Elastic Band Connected Collision Avoidance (EB-CCA) as opposed to previous work on just Elastic Band Collision Avoidance (EB-CA) by using V2X modems in the vehicles and the pedestrian's smartphone to communicate absolute position and velocity information. Note that there are many studies in the literature about Cooperative Collision Avoidance (CCA) by means of Connected Vehicles (CV) technologies. As stated in research studies, CCA systems rely on V2V (Vehicle-to-Vehicle) communications (Elbatt *et al*., 2006; Misener *et al*., 2011; Themann *et al*., 2015; Intelligent Transportation Systems Joint Program Office-Office of the Assistant Secretary for Research and Technology, 2016), Vehicle-to-Infrastructure (V2I) communications (Wang *et al*., 2008) and also on joint V2V/V2I communication technologies for cooperative collision avoidance, in order to improve road safety, avoid vehicle collisions, prevent injuries and save lives (Avanish *et al*., 2013; Gomathi *et al*., 2014).

This paper focuses on and develops the real time implementable Elastic Band Connected Collision Avoidance (EB-CCA) method to address the lack of readily implementable vehicle to pedestrian collision avoidance methods based on V2P communication in the literature. The main contributions of the paper are demonstrated using model-in-the-loop, hardware-in-the-loop simulations and experimental results.

This paper does not treat the two problems of whether the V2P communication is good enough or pedestrian detection or whether the elastic band method is good enough for pedestrian collision avoidance as separate problems. The main contribution and focus of this paper is on the combined use of V2P for pedestrian detection coupled with the use of the elastic band method for pedestrian collision avoidance. This paper concentrates on improving the elastic band pedestrian collision avoidance method where line-of-sight perception sensors fail due to a NLOS pedestrian presence.

The organization of the rest of the paper is as follows. The vehicle path following model is presented in Section 2. The experimental vehicle automation, perception and computation architecture is given in Section 3. The hardware-in-the-loop simulator used and the V2P communication setup are presented in Section 4. The Elastic Band Connected Collision Avoidance (EB-CCA) method is developed in Section 5. The parameter space based robust steering controller used in EB-CCA is given in Section 6. Hardware-in-the-loop simulation results are presented in Section 7. One exemplary field test result is used in Section 8 to demonstrate the effectiveness of the EB-CCA method proposed in this paper in a real world implementation. Vehicle behavior on relatively complex situations are presented in Section 9, followed by a field test for one of these complex scenarios in Section 10. The paper ends with conclusions in the last section.

2. VEHICLE PATH FOLLOWING MODEL

Two types of vehicle dynamics models were used in this study. A high fidelity CarSim model was used in the Hardware-in-the-Loop (HiL) simulations and is described briefly in Section 4. The linearized single track vehicle dynamics based path following model that was used in

Table 1. Parameters for the vehicle model.

β	Vehicle side slip angle (rad)	r	Vehicle yaw rate (rad/s)
Index f	Front tires	*Index r*	Rear tires
V	Vehicle velocity (m/s)	$\Delta\psi$	Yaw orientation error with respect to path at center of gravity (rad)
l_s	preview distance (m)	e_y	lateral deviation (m)
δ_f	front wheel steering angle (rad)	$\delta_r = 0$	rear wheel steering angle (rad)
J	yaw moment of inertia (3,350 kgm^2)	C_f	front cornering stiffness (19,000 N/rad)
C_r	rear cornering stiffness (19,000 N/rad)	m	vehicle mass (350 kg)
l_f	distance from CG to front axle (1.06 m)	l_r	distance from CG to rear axle (0.96 m)
l	distance parameter along path	$\rho_{ref} = 1/R$	curvature of path (1/m)

steering controller design is presented here. This linear model is illustrated in Figure 1 and the explanations of the model parameters and numerical values used are tabulated in Table 1.

The state space equation of the linearized vehicle path following model is given by

$$\begin{bmatrix} \dot{\beta} \\ \dot{r} \\ d\Delta\psi/dt \\ de_y/dt \end{bmatrix} = \begin{bmatrix} a_{11} & a_{12} & 0 & 0 \\ a_{21} & a_{22} & 0 & 0 \\ 0 & 1 & 0 & 0 \\ V & l_s & V & 0 \end{bmatrix} \begin{bmatrix} \beta \\ r \\ \Delta\psi \\ e_y \end{bmatrix} + \begin{bmatrix} b_1 \\ b_2 \\ 0 \\ 0 \end{bmatrix} \delta_f + \begin{bmatrix} 0 \\ 0 \\ -V \\ -l_s V \end{bmatrix} \rho_{ref} \quad (1)$$

where

$$a_{11} = -(C_r + C_f)/mV,\ a_{12} = -1 + (C_r l_r - C_f l_f)/mV^2$$
$$a_{21} = (C_r l_r - C_f l_f)/J,\ a_{22} = -(C_r l_r^2 + C_f l_f^2)/JV,\ b_1 = C_f/mV,\ b_2 = C_f l_f/J$$

Lateral deviation from the desired path with a preview distance of l_s is e_y as shown in Figure 1 and is calculated as

$$e_y = h + l_s \tan(\Delta\psi) \quad (2)$$

where $\Delta\psi$ is the orientation error between the vehicle longitudinal (x) axis and the desired path's tangent line and h is the lateral deviation from the desired path at the vehicle center of gravity. The aim of the steering controller is to determine and apply steering input δ_f that will result in zero tracking error e_y in the presence of road curvature ρ_{ref} while tracking the desired path. The path to be followed is obtained from a map of GPS waypoints and is usually of low curvature. If the curvature is high, the vehicle speed is reduced accordingly. The exception in this paper is when a collision risk with a pedestrian is detected and the path has to be suddenly modified to be able to avoid a collision. In that case, the resulting collision free path may have to have high curvature at relatively higher speeds.

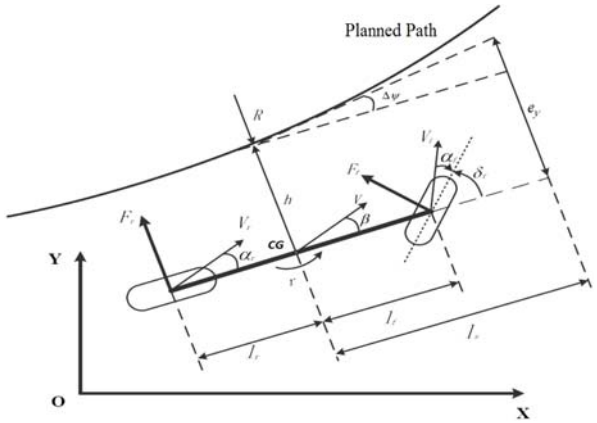

Figure 1. Single track vehicle model illustration.

In order to calculate lateral path tracking error and road curvature, our path following algorithm uses pre-calculated coefficients from a pre-determined path. Since the reference path is approximated by a sequence of third order polynomial function fits of the GPS waypoints (Emirler *et al*., 2015), the road curvature can be analytically calculated using,

$$\rho_{ref}(\lambda) = \frac{\left| \frac{dX_p(\lambda)}{d\lambda} \frac{d^2Y_p(\lambda)}{d\lambda^2} - \frac{dY_p(\lambda)}{d\lambda} \frac{d^2X_p(\lambda)}{d\lambda^2} \right|}{\left(\left(\frac{dX_p(\lambda)}{d\lambda} \right)^2 + \left(\frac{dY_p(\lambda)}{d\lambda} \right)^2 \right)^{\frac{3}{2}}} \quad (3)$$

where $X_p(l)$ and $Y_p(l)$ are the polynomial fit points on the reference path to be followed as a function of l which is non-dimensional distance along the desired path (Emirler *et al*., 2015). As the path to be followed is a sequence of third order polynomial segments and the first and second derivatives are made to match at the intersections of segments, calculation of the curvature disturbance input does not pose any numerical discontinuity problems.

3. EXPERIMENTAL VEHICLE AUTOMATION, PERCEPTION, COMPUTATION ARCHITECTURE

The vehicle used for the real-world experiments in this study is a low speed two seater fully electric shuttle (Dash

EV) which was automated in-house in our lab (Gelbal *et al.*, 2017). The automation process includes achieving drive-by-wire capability and adding sensors to gain environmental perception. To achieve drive-by-wire capability, steering, throttle and braking should be applied by actuators or electronic signals. For steering functionality, a smart electric motor was mounted and connected to the steering rack through a gear transmission mechanism that receives angular position input as the control signal over the CAN bus and rotates the steering wheel accordingly. For brake functionality, a linear electric motor is mounted behind the brake pedal that receives translational position as a control signal over the CAN bus and pulls or pushes the brake pedal accordingly. Finally, for throttle, an electronic circuit is installed to by-pass the throttle pedal potentiometer signal and replace it with our own signal.

Sensors were added after this process to handle tasks like localization and obstacle detection, thus, gaining the ability to run controllers and algorithms using these sensors and drive the vehicle autonomously. The sensors used are high accuracy GPS, Leddar sensor and 3-D LIDAR as shown in Figure 2. Our GPS sensor is a differential GPS with RTK capability. This sensor provides global location information that is used in our basic GPS waypoint map based path following application and provides 2 ~ 5 cm accuracy in the RTK mode. It can provide heading information even when the vehicle is stationary. The Leddar sensor is a cheap solid state LIDAR that provides distance information about the obstacles in front of the vehicle. It scans a field of view of 95° and detects obstacle distances in one plane. In this study, it is mainly used as an additional emergency measure. It detects obstacles in front and that information is used to decide if there is any obstacle very close that creates a need of emergency slow-down or stop.

The LIDAR, camera and Leddar are the perception sensors we typically use in an experimental vehicle that works in conjunction with the V2P communication based pedestrian detection. These perception sensors including the Leddar sensor continuously scan the environment for obstacles/pedestrians. The current V2P and Leddar integration in the experiment in the paper is rule based, i.e. the Leddar (perception) sensor and V2P detections are compared with each other to categorize the pedestrian as line-of-sight or non-line-of-sight.

Our LIDAR is a 360° 16 plane Velodyne puck unit which scans the vehicle's environment and translates it into a 3D point cloud. Due to high resolution and wide field of view, this sensor provides significant advantage over Leddar and is used in our numerous applications like SLAM, map matching, obstacle avoidance and object classification. We also have a PointGrey camera and a Mobileye camera that we can add to this vehicle when needed. Besides these localization and perception sensors, our vehicles also have DSRC radio units which communicate with other vehicles, instrumented traffic lights, road side unit broadcasted traffic sign information and DSRC enabled smartphones.

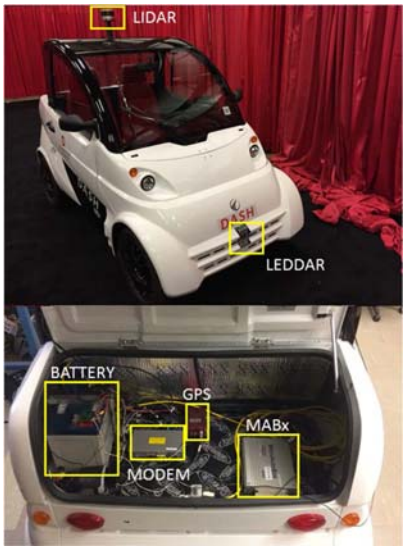

Figure 2. Equipment on the vehicle.

It is important to note that some experiments that were similar to those reported in this study, took place at night due to other reasons and no problems were experienced in the EB-CCA method and V2P communication with night time situations. However, we experienced line-of-sight pedestrian detection problems with our camera during night time situations. Based on previous experience and the available literature, LIDAR and Leddar do not have problems at night but do not operate at their best during rain and fog.

The element between the actuators and sensors and DSRC radio is the dSPACE MicroAutoBox (MABx) electronic control unit that is widely used in this field for rapid controller prototyping. Simulink is used to create algorithms and controllers for autonomous driving and the model is embedded into the MicroAutoBox using automatic code generation. The MicroAutoBox unit receives data from sensors on the vehicle through the connection of UDP or CAN depending on the sensor. This sensor data is used in the controllers and algorithms running in MicroAutoBox. Then, outputs of these controllers are carried on to actuators through physical connection of the I/O or CAN ports of the MicroAutoBox to the corresponding port of the actuator. All of the sensors, actuators and the processing unit MicroAutoBox are powered by the 12 V battery in the trunk of the vehicle. Some of the equipment explained are shown in the vehicle pictures of Figure 2.

4. HIL SIMULATOR AND V2P COMMUNICATION SETUP

4.1. HIL Simulator

Along with the single track vehicle model for controller

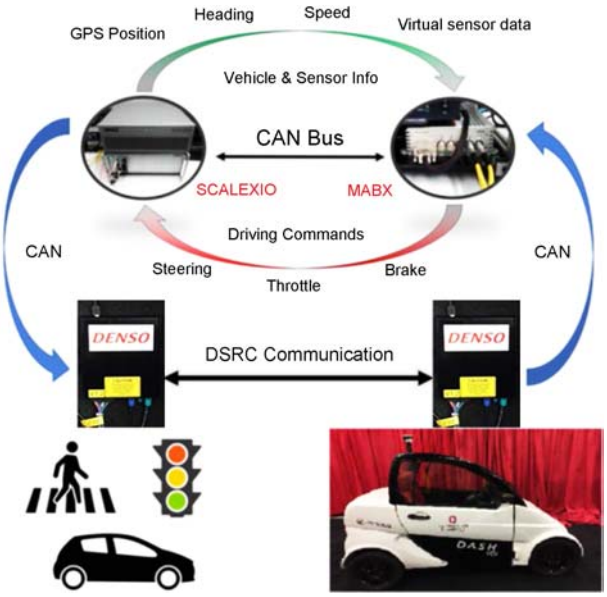

Figure 3. HIL elements and communication.

design and an autonomous vehicle for real world testing, we also have a Hardware-in-the-Loop (HiL) simulator which we use to realistically test our controllers and algorithms before implementing them on the real vehicle. We have CarSim and Simulink as software, dSPACE SCALEXIO and MicroAutoBox (shown as MABx in Figure 2) and two DSRC radio units as hardware in the HiL simulator as shown in Figure 3. SCALEXIO is essentially a fast computer that runs a Simulink model with a CarSim vehicle dynamics block that represents the autonomous vehicle dynamics. CarSim is a high fidelity vehicle dynamics modeling and simulation software that allows us to simulate realistic vehicle dynamics models in real time. Actuator inputs and sensor outputs of this vehicle are connected to the CAN bus which is shared with the MicroAutoBox. Through this bus, the MicroAutoBox can receive sensor and vehicle data and send control signals to actuate the steering, brake and throttle of the vehicle, working as if it is connected to the real vehicle. SCALEXIO receives these control signals and uses them as an input for the vehicle dynamics calculations. The HiL simulator elements and communication between HiL elements are illustrated in Figure 3.

The HiL simulator is capable of calculating high fidelity dynamics in real time using the experimental vehicle's parameters, capable of controlling the vehicle using a MicroAutoBox electronic control unit just as in the actual autonomous vehicle. Also, with CarSim, we can make use of various kinds of scenario elements for simulating different situations such as traffic lights, other signs on the road, other vehicles and pedestrians modeled as kinematic objects.

Moreover, these elements can communicate with the autonomous vehicle using V2X communication over the

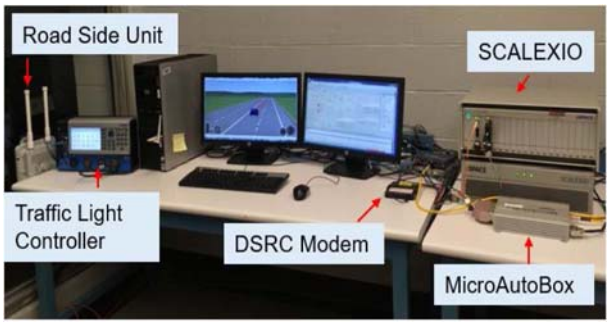

Figure 4. HIL equipment.

DSRC radio channel. Vehicles use V2V messages, infrastructure uses V2I messages and pedestrians use V2P messages, respectively using standard message formats from SAE J2735 DSRC message set dictionary. This realistic simulation environment is a significant advantage for testing numerous scenarios repeatedly and doing adjustments and optimizations on controllers or algorithms before implementing them in a real vehicle and conducting real experiments. After those adjustments, the resulting controllers or algorithms can be used on the real vehicle with very few or no modifications. A photo of the HiL simulator in our lab is shown in Figure 4.

5. ELASTIC BAND CONNECTED COLLISION AVOIDANCE (EB-CCA) METHOD

5.1. Path Modification with Elastic Band

After the position of the pedestrian is obtained via V2P communication, an alternative, collision free path to be followed is created if a collision is imminent. Since the vehicle is a non-holonomic system, an ideal maneuver would be when the path smoothly deviates towards the avoidance direction and smoothly connects back to the pre-determined path. This makes it much easier for the vehicle to apply the maneuver from vehicle dynamics perspective. As a result, without exerting unnecessary lateral forces, avoidance maneuver is more stable and feels more comfortable for the passengers. The Elastic Band algorithm achieves these conditions with a relatively small time of computation and Cooperativeness comes from the communication between vehicle and the pedestrian, which solves lots of high crash risk NLOS situations. This is the main reason EB-CCA method was chosen. Therefore, the path is created by modifying the existing points on the path according to the position of the pedestrian. Our path modification algorithm is based on the elastic band theory (Ararat and Aksun-Guvenc, 2008; Emirler *et al*., 2016), where socially acceptable distance is also considered in modifying the deformed path (Wang *et al*., 2018). EB-CCA was chosen for real time path modification here as the elastic band method can be applied naturally to a road vehicle path following task where there is a pre-defined path that lies between the lanes with collision avoidance

Table 2. Advantages and disadvantages for some path planning methods.

Method	Advantages	Disadvantages	Computation time
Motion primitives	Very simple and very fast.	Route is neither optimal nor flexible. Behavior can be unnatural for a car.	Low
Rapidly-exploring random tree	Easy to implement. Suitable for holonomic kinematics.	Multiple random searches are relatively time consuming. Can cause unnatural behavior for a car due to randomness.	High
Model predictive control	On-line path generation and modification are combined.	With constraints and weights, calculation of optimization is relatively slow.	High
Elastic band	Modified path is well defined and structured. Transition from or to the non-modified path is natural. Calculation is relatively fast.	Relies on a different algorithm for generation of pre-determined path.	Medium

maneuvering being limited at most to emergency (sudden) lane changes. This fits the elastic-band framework naturally as the pre-defined path is the undeformed elastic band and the emergency maneuver trajectory can easily be created by deforming the band. Another reason is the real-time computation capability. Some of the advantages and disadvantages for different path planning algorithms are shown in Table 2.

The elastic band method is applicable to both highway usage and small areas with high pedestrian density. This paper concentrates on urban, i.e. low speed inside the city, driving on public roads typical of a university campus environment. The method is able to consider vehicles on other lanes and can perform satisfactory lane changes at higher speeds also.

In elastic band theory, the initial path is deformed by internal and external forces acting on the band which represents the vehicle path. Internal forces are spring forces which hold the band or the path together while external forces keep the band or path away from the pedestrian like artificial potential field forces. Figure 5 shows an initial path displayed as an elastic band which is deformed by both internal and external forces in the presence of a pedestrian.

The elastic band is a sequence of displaceable nodes denoted by N_i in Figure 5 that initially correspond to the original local path of the autonomous shuttle in the vicinity of the detected pedestrian. The initial positions of the nodes N_i with respect to the pedestrian are shown by position vectors r_i. Internal forces are formulated by adding springs with stiffness k_s and spring force F_{int} acting on node i due to the adjacent nodes N_j with $j = i + 1$ or $j = i - 1$ for $I = 1, 2,\ldots, n$. The function of internal forces is to hold the nodes or the local path together as a displaceable part of the route of the autonomous shuttle as shown in Figure 5. External forces are defined once a pedestrian is detected to deform the band and hence the local path away from the pedestrian like artificial potential field forces. The external forces keep deforming the local path around the pedestrian who may be moving while the internal forces keep the nodes together in the form of a collision free path to be followed. $\boldsymbol{u}_i$ for $i = 1, 2,\ldots, n$ are the deformations of the nodes under the action of external and internal forces when a pedestrian is detected. The internal forces $\mathbf{F}_{i,j}^{int}$ become $\mathbf{F}_{i,j}^{int^*}$ after the deformation of the local path. After a pedestrian is detected, external forces are applied and the nodes of the deformed path become the new positions $\boldsymbol{r}_i + \boldsymbol{u}_i$ for $i = 1, 2,\ldots, n$ as determined by the balance of internal and external forces acting on the nodes.

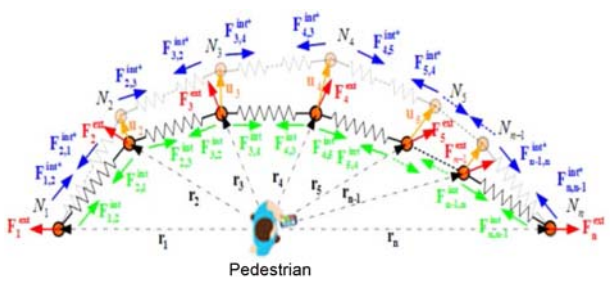

Figure 5. Initial path deformed by internal and external forces in the presence of a pedestrian on the path.

The static balance of internal forces acting on node N_i in Figure 5 before a pedestrian is detected are

$$\mathbf{F}_{i,i-1}^{int} + \mathbf{F}_{i,i+1}^{int} = k_s(\mathbf{r}_{i-1} - \mathbf{r}_i) + k_s(\mathbf{r}_{i+1} - \mathbf{r}_i) = 0 \quad (4)$$

After the pedestrian is detected and external forces are applied and the static balance of internal and external forces acting on node N_i in Figure 5 become

$$\begin{aligned}\mathbf{F}_{i,i-1}^{int^*} + \mathbf{F}_{i,i+1}^{int^*} + \mathbf{F}_i^{ext} &= k_s(\mathbf{r}_{i-1} + \mathbf{u}_{i-1} - (\mathbf{r}_i + \mathbf{u}_i)) \\ &+ k_s(\mathbf{r}_{i+1} + \mathbf{u}_{i+1} - (\mathbf{r}_i + \mathbf{u}_i)) + \mathbf{F}_i^{ext} = 0\end{aligned} \quad (5)$$

which using the identity in Equation (4) becomes

$$\mathbf{F}_i^{ext} = -\left[k_s(\mathbf{u}_{i-1} - \mathbf{u}_i) + k_s(\mathbf{u}_{i+1} - \mathbf{u}_i)\right] = -k_s(\mathbf{u}_{i-1} - 2\mathbf{u}_i + \mathbf{u}_{i+1}) \quad (6)$$

The external force $\mathbf{F}_i^{ext}$ acting on node N_i is calculated as a repulsive force using

$$\mathbf{F}_{\mathbf{i}}^{\mathbf{ext}} = \begin{cases} (\mathbf{F}_{\mathbf{i}}^{\mathbf{ext}})_{\max}, & |\mathbf{r}_{\mathbf{i}}| < d \\ -k_{\mathrm{e}}(|\mathbf{r}_{\mathbf{i}}| - r_{\max})\dfrac{\mathbf{r}_{\mathbf{i}}}{|\mathbf{r}_{\mathbf{i}}|}, & d \le |\mathbf{r}_{\mathbf{i}}| \le r_{\max}, \\ 0, & |\mathbf{r}_{\mathbf{i}}| > r_{\max} \end{cases} \quad (7)$$

where $|\cdots|$ denotes the magnitude of the argument. $(\mathbf{F}_{\mathbf{i}}^{\mathbf{ext}})_{\max}$ in Equation (7) is used to saturate the repulsive force within $|\mathbf{r}_{\mathbf{i}}| < d$ so that it does not go to infinity as $|\mathbf{r}_{\mathbf{i}}| \to 0$. k_{e} is the stiffness associated with the repulsive force and $r_{\max}$ is the range of the repulsive force. Once a pedestrian is detected and localized with respect to the path of the vehicle using V2P communication, Equations (6) and (7) are solved to obtain the new coordinates $\boldsymbol{r}_{\mathbf{i}} + \boldsymbol{u}_{\mathbf{i}}$ for $i = 1, 2, \ldots, n$ of the locally deformed path. In the case of a moving pedestrian, the computations are repeated at each time step to continue to locally deform the obstacle avoidance path to be followed. This provides a new modified path for the corresponding position of the pedestrian in that timestep. Moreover, this calculation can be applied for multiple times to modify the path further for each object present and desired to be avoided, such as multiple pedestrians away from each other. When there are multiple pedestrians and they are close to each other, however, a basic decision-making algorithm, based on the position and velocity comparison, takes them into account as one moving object with a bigger radius.

The distance d in Equation (7) is also used to model the physical dimension of the autonomous vehicle d_{vehicle}. Noting that $|\mathbf{r}_{\mathbf{i}}| < d$ is a circular region around the pedestrian to be avoided, d is adjusted such the pedestrian stays within that region during any short duration relative displacement and the V2P communication delay of the car within the detection sampling instants. In the case of a moving pedestrian, the circular region $|\mathbf{r}_{\mathbf{i}}| < d$ keeps moving with the pedestrian, requiring the local path modification calculations based on solving Equations (6) and (7) to take place within the steering control sampling time.

In socially acceptable collision avoidance (Wang *et al*., 2018), the circular region $|\mathbf{r}_{\mathbf{i}}| < d$ is increased to also accommodate a pedestrian socially acceptable distance of about 1.5 m. This distance is chosen as a comfortable base value and may vary between countries, depending on the personal space needs (Sorokowska *et al.*, 2017). Therefore, it was implemented as a parameter and can be adjusted. d is calculated using

$$d = d_{\mathrm{vehicle}} + d_{\mathrm{pedestrians}} + d_{\mathrm{social}}, \quad (8)$$

where d_{vehicle}, $d_{\mathrm{pedestrian}}$ and d_{social} account for the autonomous vehicle dimensions, the pedestrian possible motion between two V2P detection sampling instances and the social acceptance distance for pedestrians. A maximum possible pedestrian speed of 1.5 m/sec is used in computing $d_{\mathrm{pedestrian}}$. In the current experiments and simulations, this distance is preferred to be kept at its maximum value according to the pedestrian speed for safety and can be adjusted to a smaller radius for lower speed pedestrians or higher radius for higher speed vulnerable road users, if desired.

5.2. Following the Modified Path

A preview distance of 15 m to the V2P detected pedestrian is used in the HiL simulations and experiment here to modify the path based on the elastic band method of the previous sub-section. After modification of the points on the path with the elastic band method, the modified path should be followed instead of the actual path. Our past work involved fitting several segments of cubic polynomials to the deformed elastic band nodes. This method was implemented in real time for a stationary pedestrian in our previous work. However, this approach limited our real time computation speed for moving pedestrians where the curve fits had to be repeated at each time instant. For this reason, a simpler method for following the modified path with a point to point approach is formulated and used here. This method runs much faster since it uses a much faster computation to determine lateral deviation at each node. This method is illustrated in Figure 6.

In our new approach, the orthogonal distance to the line between two deformed nodes, which are the closest to the vehicle are calculated as shown in Figure 6. This distance is considered to be the lateral error for the modified path and used as the source of the lateral error for the steering controller when there is a need to avoid the pedestrian. Calculation for a full elastic band method modified path consisting of 500 nodes and one pedestrian takes approximately 20 ms for one step while this time was approximately 200 ms for our previous method that used cubic curve fitting as explained in Emirler *et al*. (2015). The lateral error e_{y} for this method after the V2P based detection of a pedestrian on the path within the 15 m preview distance is

$$e_{\mathrm{y}} = \frac{\det\left(\begin{bmatrix} a \\ b \end{bmatrix}\right)}{\|a\|} \quad (9)$$

$$a = P_2 - P_1 \quad (10)$$

$$b = P_{\mathrm{v}} - P_1 \quad (11)$$

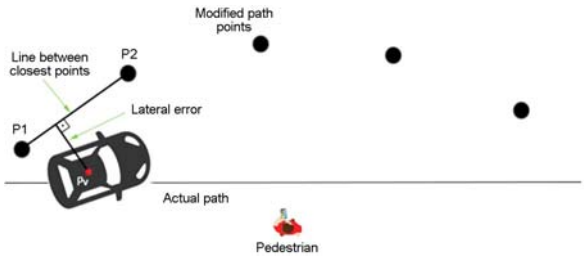

Figure 6. Lateral error calculation for pedestrian collision avoidance.

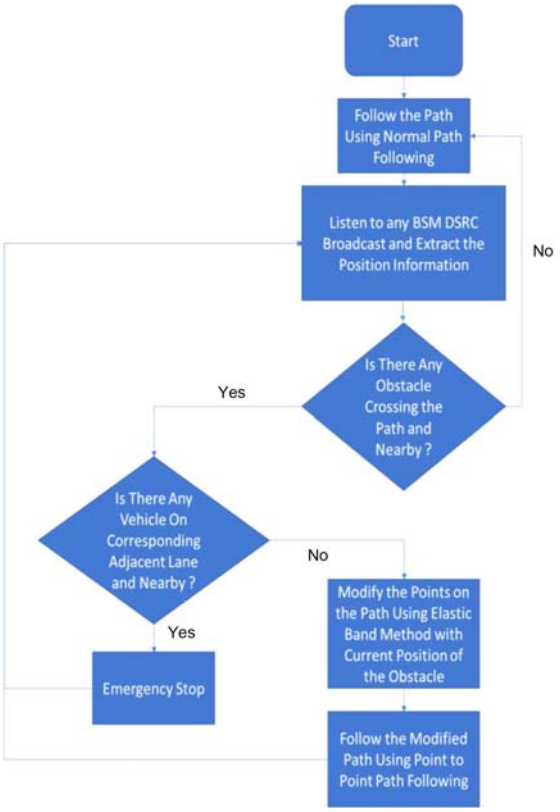

Figure 7. Flowchart of the algorithm.

where a and b are row vectors calculated from Euclidean coordinates of closest points P_1, P_2 and vehicle's coordinate P_v. $\|a\|$ is the length of the vector a. This calculation is done at every step that needs obstacle avoidance behavior when there is a V2P detected pedestrian who is nearby. There is also the possibility of the presence of other vehicles on adjacent lanes when a maneuver is intended. For such cases, vehicle presence on the corresponding lane should be observed before starting the maneuver. This can be done using a sensor such as LIDAR, or through an algorithm that considers the other vehicles' information obtained by V2V communication. A flowchart that presents the steps of the overall algorithm and decision making is shown in Figure 7.

6. STEERING CONTROL

The low-level feedback control system architecture with the EB-CCA algorithm for pedestrian and car collision avoidance using V2P communication is shown in Figure 8. A longitudinal speed controller follows the desired speed profile while a lateral steering controller navigates the vehicle through a path of GPS waypoints extracted from a map. If the vehicle OBU DSRC detects a possible collision with a nearby pedestrian through V2P communication, the EB-CCA method of Section 5 is used to follow the

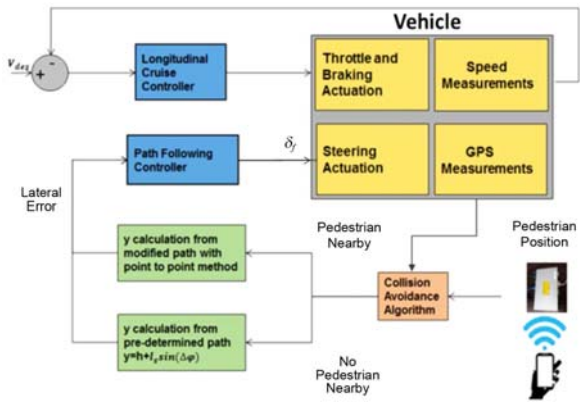

Figure 8. Low level control loops.

deformed collision free path. The steering controller handles both the ordinary steering tasks and the sudden collision avoidance maneuvering tasks. It is possible to design and use a more aggressive steering controller during the collision avoidance maneuver. However, this was not necessary in the simulations and experiment here and a single steering controller was used for both path tracking and collision avoidance.

A robust PD feedback steering controller is designed using the parameter space approach. The D-stability region that is used for constraining the closed loop poles to satisfy settling time, damping ratio and bandwidth specifications is shown in Figure 9. The K_d-K_p controller parameter solution region which satisfies the D-stability requirements is shown in Figure 10. The D-stability region is chosen by assuming the settling time constraint to be $\sigma = 0.3$, a minimum damping ratio corresponding to $\theta = 45°$ is determined as 0.707, and a bandwidth constraint of natural frequency $\omega_n = 5$ rad/sec. The overall solution region of Figure 10 shows the Real Root (RRB) and Complex Root (CRB) boundaries which correspond to the steering controllers which can also use preview of the trajectory ahead in a feedforward controller. We have also used MPC based steering control in some of our previous work. As the

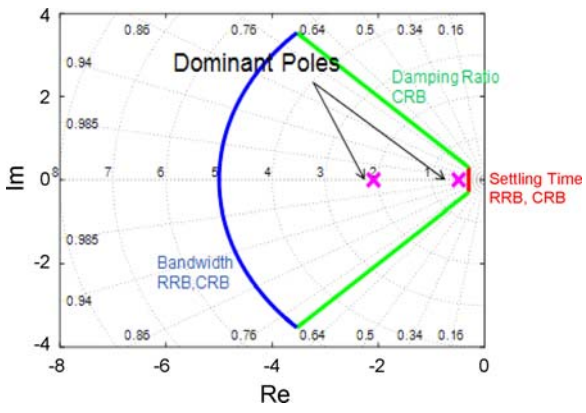

Figure 9. D-stability region in complex plain.

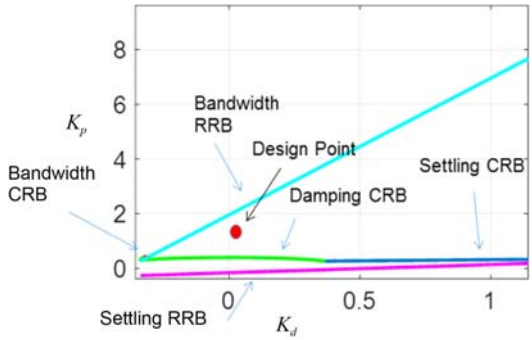

Figure 10. D-stability solution region.

current paper focuses more on the collision avoidance method and the use of V2P communication to obtain more information about the presence of pedestrians, we used a parameter space based robust PID steering controller here. Once the deformed collision free trajectory is obtained, it is also possible to use an MPC steering controller to follow it autonomously. It is possible to add constraints and weights to the MPC problem for avoiding collision with obstacles. The reason that we have not used an MPC steering controller or an MPC steering controller that also avoids obstacles in this paper is that MPC computations are too demanding for real time implementation and the proposed method executes much faster.

7. HARDWARE IN THE LOOP SIMULATION STUDY

7.1. Scenarios

In order to test the algorithm in a realistic environment, the HiL system that was discussed in Section 4 is used. One of the modems was used for representing the DSRC enabled smartphone of a pedestrian and broadcasted the position information of the pedestrian. The other modem was used for representing the OBU modem in the vehicle as it received the pedestrian position information and sent it to the MicroAutoBox control unit. This V2P communication is illustrated in Figure 11. The MicroAutoBox control unit was configured to receive these messages and control the vehicle inside the simulation while running the algorithm in real-time.

Two actual DSRC devices, one for the vehicle and one for the pedestrian info, is used in the HiL setup so that a model is not necessary. A soft GPS sensor is used in the HiL simulator. The accuracy of the soft GPS sensor can be adjusted and corresponds to the real GPS/IMU sensor on the vehicle with an accuracy of 2 cm in RTK mode. The latency/packet-drop-rate of the DSRC was not considered in the paper in model-in-the-loop simulations and it was the latency/packet-drop rate of the actual DSRC devices used in the hardware-in-the-loop and experimental vehicle road evaluations. All hardware-in-the-loop and vehicle experiments are real time meaning that the collision

Figure 11. V2P communication in HiL simulation scenarios.

avoidance path modification computations should be carried out fast enough to be executed as the vehicle and pedestrians are moving.

Under these assumptions and using this HiL setup, several scenarios were derived from the five priority pre-crash scenarios selected by U.S. DOT. In these five scenarios, three distinct vehicle maneuvers and three distinct pedestrian maneuvers which are vehicle going straight, vehicle turning right, vehicle turning left, pedestrian crossing, pedestrian on the road, and pedestrian walking adjacent to the road were identified (Swanson *et al*., 2016). Vehicle turning right and turning left were combined into one vehicle turning scenario and a total of 4 scenarios were simulated. Illustrations of these scenarios which were created in CarSim are shown in Figure 12, where the number at the bottom left of each box represents the number of the scenario. Scenarios 1 and 4 are non-line of sight (NLOS) cases in which the pedestrian is hidden behind a car or a building. Pedestrians were scaled up in

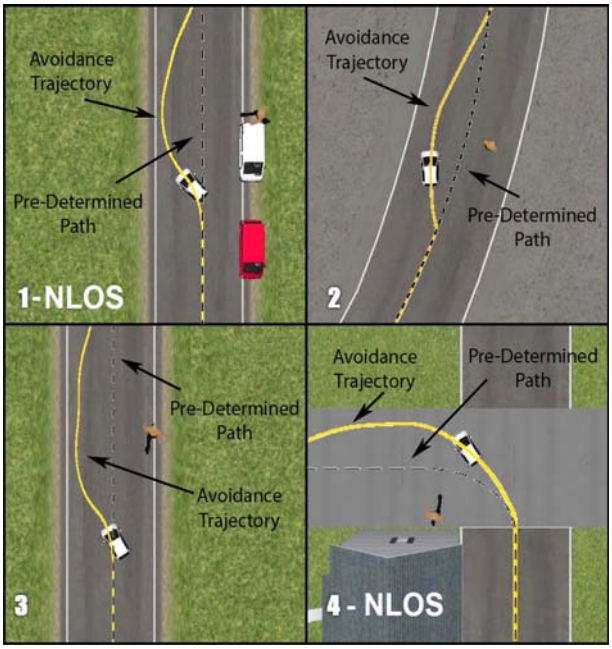

Figure 12. Priority pre-crash scenarios illustrated in CarSim.

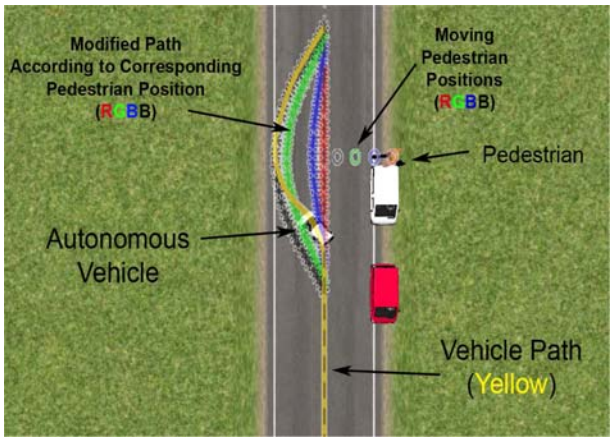

Figure 13. Notation for simulation result demonstration.

size to increase visibility in figures. Roads are assumed wide enough to avoid the pedestrian with at least the socially acceptable distance. It is also important to note that the pedestrian model for the simulations is a basic linear one directional motion model with constant speed. Complex pedestrian behavior is currently not studied in this work. However, if desired, complex behavior analysis methods can be easily combined with this method after running them as a separate algorithm.

The notation used in the graphs of the results for the simulations is illustrated in Figure 13. Moving pedestrian position in time is represented by circle shapes which are colored in red, green, blue, black, while the corresponding modified path points corresponding to each instance of pedestrian position are represented in the same color by asterisk shape. The final dynamically modified vehicle path is represented by the yellow colored line and the path before deformation is represented by the black dotted line. During the HiL simulation the vehicle follows the yellow path.

7.1.1. Vehicle going straight and pedestrian crossing the road

In this NLOS scenario, while the vehicle is moving forward on the path, suddenly a pedestrian tries to cross the road. This scenario is the most frequent pre-crash scenario. According to the U.S. DOT report, highest rates of pedestrian crashes happen in situations where the pedestrian is crossing the road and highest rates of fatalities involved vehicles that were going straight. Moreover, in our case, there are also vehicles parked on the right side of the road which is also the side the pedestrian comes from. These vehicles block the view of the ego vehicle making it unable to detect the pedestrian with perception sensors because of the NLOS situation. The vehicle is able to avoid collision while moving forward at a speed of 25 km/h and the pedestrian is moving across the road at a speed of 1 m/s. While the pedestrian is walking across the road, a new modified path is calculated at each step for the current

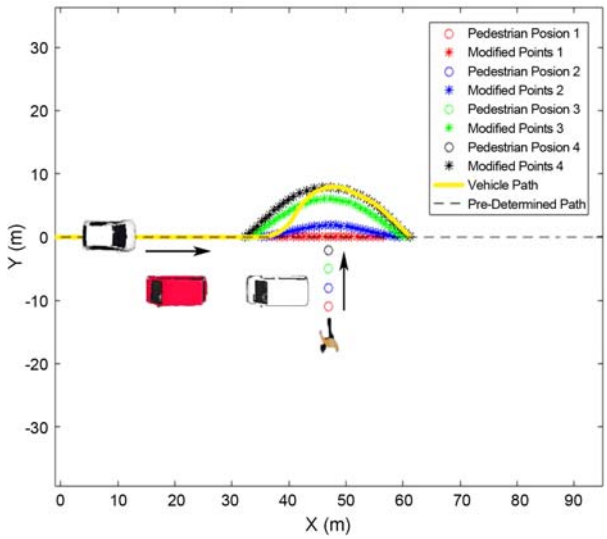

Figure 14. HiL simulation results for the first scenario.

position of the pedestrian. Some of the points the pedestrian passes while walking and corresponding modified paths are shown in Figure 14 together with the final path that the vehicle follows in response to the pedestrian motion. The autonomous vehicle and moving pedestrian are illustrated in Figure 14 during this maneuver as well as the vehicles parked next to the road. These parked vehicles create the NLOS situation. Direction of movement for the autonomous vehicle and pedestrian are also illustrated using black arrows. Illustrated objects in Figure 14 and the other figures are drawn larger as compared to their real dimensions to increase their visibility. As the pedestrian moves closer to the vehicle, the vehicle's deformed path moves further away to keep the desired distance.

7.1.2. Vehicle going straight with pedestrian on the road

This scenario consists of a forward moving vehicle and a pedestrian standing on the road. The environment is a parking lot. In order to use this scenario in real world experiments, GPS points of the path were collected from our lab's parking lot. The pedestrian is standing on the road while he is busy and unaware of the vehicle coming closer. We are assuming that weather and/or lighting conditions (fog, rain etc.) do not allow the perception sensors to detect the pedestrian in a reliable manner. V2P communication is, then, the only way to avoid colliding with the pedestrian. Also, different from the other scenarios, the vehicle moves at a speed of 10 km/h. The HiL simulation results are shown in Figure 15. The autonomous vehicle and the standing pedestrian are also illustrated in this figure. Direction of movement for the autonomous vehicle is shown with a black arrow. The EB-CCA method is able to easily determine and execute a collision free maneuver as seen in Figure 15.

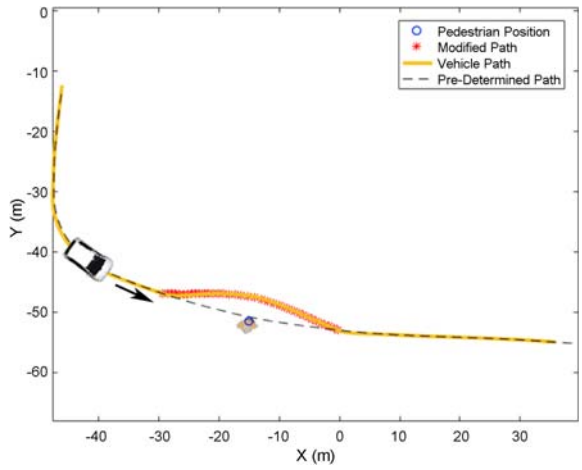

Figure 15. HiL simulation results for second scenario.

7.1.3. Vehicle going straight and pedestrian walking adjacent to the road

Similar to the first scenario, a straight road is used in this scenario where the vehicle is travelling forward at a speed of 25 km/h. There is a pedestrian walking on the side of the road. For this scenario, we are assuming weather conditions are not allowing any of the perception sensors to reliably detect the pedestrian. Therefore, the vehicle relies only on the position information it receives from V2P communication to avoid colliding with the pedestrian. Simulation results are shown in Figure 16. It is seen from the vehicle path that modified points are constantly changing with the motion of the pedestrian. The vehicle path for different locations of the pedestrian and the vehicle path for the moving pedestrian are shown in Figure 16. The direction of movement for the autonomous vehicle and pedestrian are shown with black arrows. The behavior of the vehicle can be observed and generalized to any

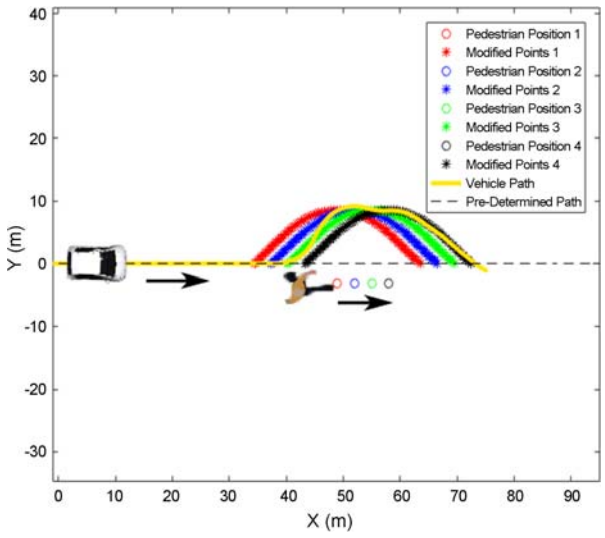

Figure 16. HiL simulation results for the third scenario.

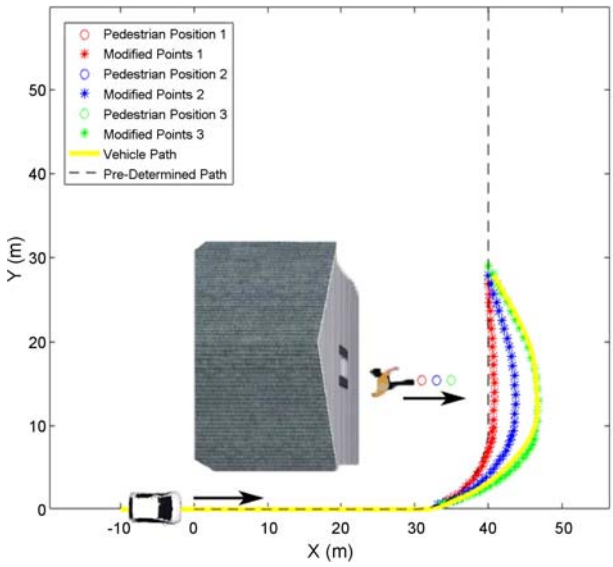

Figure 17. HiL simulation results for the fourth scenario.

situation that involves a pedestrian moving towards the same direction as the vehicle.

7.1.4. Vehicle turning left and pedestrian crossing the road

In this NLOS scenario, the vehicle will turn left while a pedestrian is trying to cross the road just around the corner. According to the U.S. DOT report, crashes for this type of scenario occur in adverse weather conditions, although these crashes may have a rare death rate. Additionally, there is a building right at the corner of the road and perception sensors cannot detect the pedestrian because of the NLOS situation caused by the building. Since the ego vehicle has a DSRC radio unit and the pedestrian has a smartphone with DSRC capability, the method presented in this paper will work in avoiding a collision. Note that DSRC communication is also disturbed by the building. But the packet delivery rate at this distance with a couple of walls is still sufficient for the vehicle to know that there is a pedestrian. The vehicle is moving at a speed of 25 km/h. The HiL simulation results in Figure 17 show the elastic band path being followed for several different locations of the pedestrian and the path for the moving pedestrian.

7.2. Evaluation

For all of the scenarios, lateral error calculated by the pedestrian avoidance algorithm is shown in Figure 18 with the scenario number on the y axis labels. Time on the graph for each scenario is starting from the time that a nearby pedestrian is detected and ending at the time the pedestrian is far behind. Lateral path modification error calculation has a value only for this time period, otherwise it is zero. While the vehicle is performing the collision avoidance maneuver, path following method switches to a point to point based path following, as explained in the Section 5.2. Therefore, while following the modified path, there are

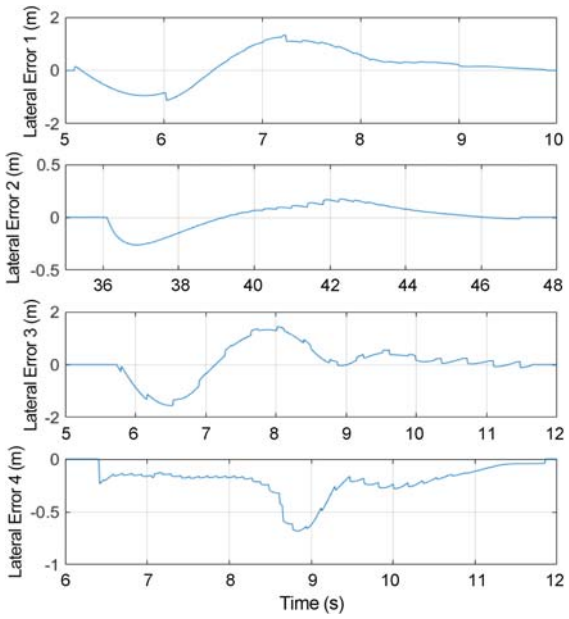

Figure 18. Lateral error vs time graphs of HiL simulations.

Table 3. RMS lateral error values for simulations.

Scenario	Vehicle Speed (km/h)	Pedestrian Speed (m/s)	RMS Value of Lateral Error (m)
1	25	1	0.6538
2	10	0	0.0459
3	25	1	0.5693
4	25	0.5	0.1923

small jumps seen in the error, where calculation switches to the next point. An RMS error table is created in Table 3 for different vehicle and pedestrian speed values for each scenario. Zero error parts on left and right side (when there is no pedestrian nearby) are not taken into consideration while calculating RMS values.

8. FIELD TEST RESULTS FOR SCENARIO 2

In addition to HiL simulations, the second scenario in Section 7 was tested by using our Dash EV experimental autonomous vehicle presented earlier in the paper. Using the same GPS points as in the second scenario, a pre-determined path was generated. A DSRC road side unit was prepared using one of the DSRC modems, a laptop and a power supply for the modem. This modem which also corresponds to the stationary pedestrian, was programmed to broadcast its GPS position through DSRC within a PSM packet. The pedestrian is a non-moving object in this case, which also corresponds to static pedestrian in HiL Simulation of the scenario 2. The road side unit representing the pedestrian with a DSRC enabled smartphone is shown in Figure 19 together with a photo taken during the experiment.

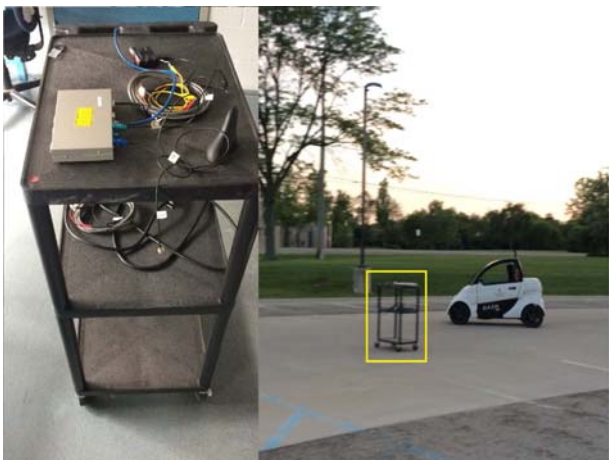

Figure 19. DSRC unit representing the pedestrian.

The DSRC radio unit's communication range is up to 1 km for Line-of-Sight (LOS) conditions. They can communicate with each other even when there is a building between them (NLOS condition) and under extreme weather conditions. Since our starting point is within the 1 km range and there was no NLOS condition, communication was clear from the start and the autonomous vehicle was receiving position data from the pedestrian unit. As seen in the experimental EB-CCA results in Figure 20, the real vehicle was able to calculate the elastic band corrections in real-time and was also able to follow the modified path very close to the HiL simulation result. These results demonstrate the effectiveness of the V2P communication based EB-CCA method for avoiding crashes between cars and pedestrians when perception sensors have difficulty in pedestrian detection.

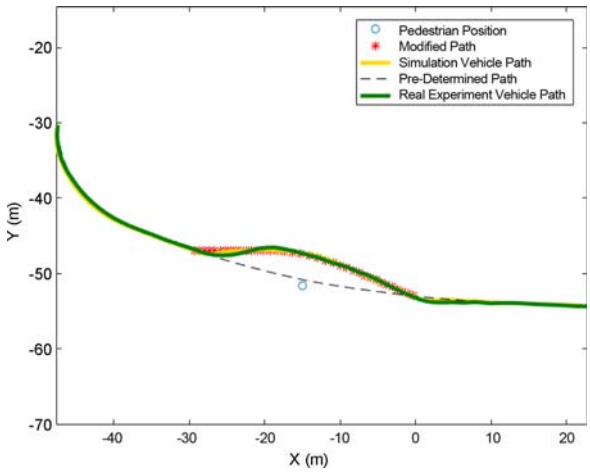

Figure 20. Real world experiment results with simulation results.

9. SIMULATIONS FOR COMPLEX SCENARIOS

9.1. Scenarios and Results

Other than scenarios that are obtained from U.S. DOT statistics with high crash possibility, three additional scenarios were simulated in the HiL simulator to demonstrate the vehicle behavior in relatively complex cases such as presence of multiple pedestrians or higher vehicle speed. In the first scenario, there are two pedestrians who are away from each other and they are trying to cross the road from different sides of the vehicle. The vehicle's original path is a straight line and passes between the pedestrians. During the HiL simulation, the EB-CCA method modified the path to accommodate the motion of the pedestrians as shown in Figure 21. This scenario demonstrates the behavior of the vehicle when there are multiple pedestrians away from each other on different sides of the vehicle. The path is modified for each pedestrian.

In the second scenario, there are multiple pedestrians but this time they are near each other and they walk together. Since the pedestrian model is basic as discussed previously, a simple decision-making algorithm decides if these are moving together by comparing their speeds and positions. After deciding that the pedestrians move together, they are considered as a single pedestrian cluster with a larger radius and the EB-CCA algorithm is applied according to that consideration. The results are shown in Figure 22, with

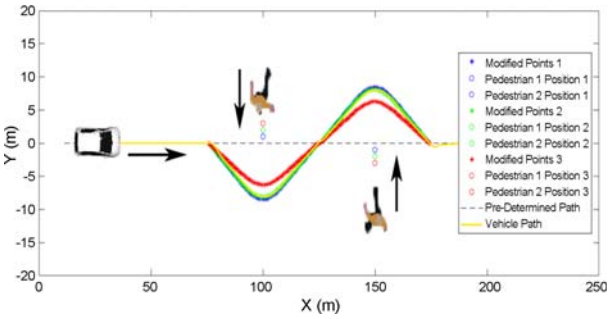

Figure 21. HiL simulation results for multiple pedestrians first scenario.

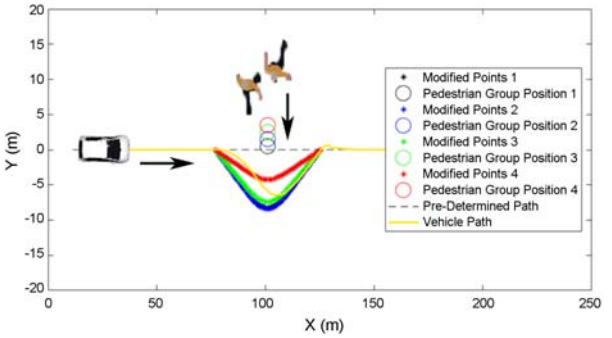

Figure 22. HiL simulation results for multiple pedestrians second scenario.

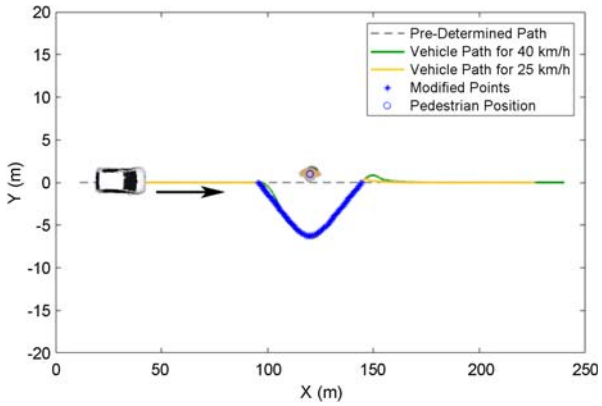

Figure 23. HiL simulation results for higher vehicle speed.

illustration of the vehicle and two pedestrians walking as a group. Black arrows indicate the direction of the movement for the vehicle and group of pedestrians. This scenario demonstrates the behavior of the vehicle when there are multiple pedestrians close to each other and moving together in the same direction. The EB-CCA algorithm treats them as a single obstacle with a larger radius and modifies the vehicle path accordingly.

The third scenario mainly addresses the high vehicle speed case. Two different simulations are conducted for this scenario for two different vehicle speeds and the pedestrian is static in both of them. The results are shown in Figure 23. It is seen that the algorithm still works reliably in higher speeds. The vehicle in this study is not legally allowed to go up to higher speeds.

10. FIELD TEST FOR A COMPLEX SCENARIO

After simulations, a field test for a complex scenario has been conducted. A grass field was chosen for the experiments because of the wide available area for safety. Two pedestrian groups were placed to stand in two different places near the vehicle path to represent the multiple pedestrian groups case. There is also a vehicle parked next to a pedestrian group which represents the NLOS case. The pedestrians have hand-held portable DSRC units (that can communicate with their smartphones using Bluetooth communication). The autonomous vehicle is aware of the pedestrian locations through V2P communication using PSM. The scene at the beginning of the experiment is shown in the top left corner of Figure 24 and is marked as 1. The parts that are labeled as 2, 3 and 4 in Figure 24 correspond to subsequent snapshots of the motion of the vehicle during the obstacle avoidance maneuver.

The undeformed path for the vehicle was constructed from the GPS points which are collected by driving the vehicle manually in the absence of the other car and pedestrians and is shown as the pre-determined path in Figure 25. The experimental vehicle was driven

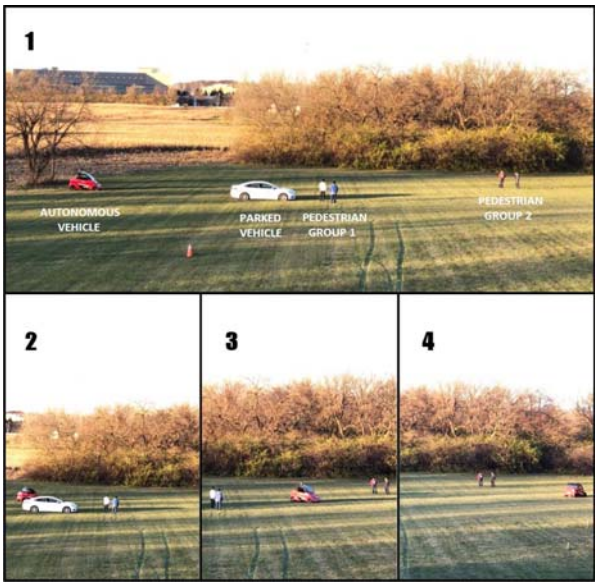

Figure 24. Illustration of the experiment.

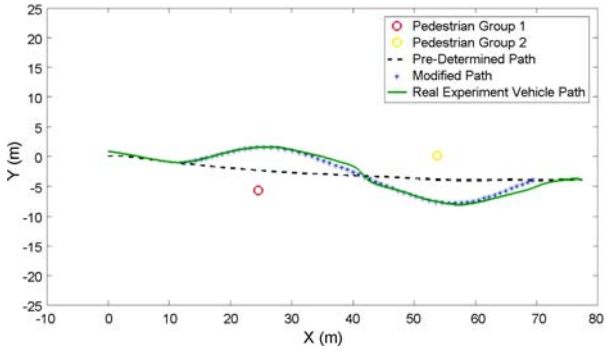

Figure 25. Experiment results.

autonomously during the test. While the experimental vehicle does path following, it also calculates the modified path in real time according to the locations of the pedestrian groups (and the location of the other car) and performs the maneuver. Along with the pre-determined path; the modified path, the two pedestrian group positions and the computed and actual vehicle trajectories are also shown in Figure 25. It is seen that the EB-CCA algorithm is able to calculate the modified path in real time for multiple pedestrians and perform the obstacle avoidance maneuver satisfactorily. In spite of the negative effect of the terrain on vehicle motion and steering, the vehicle was still able to avoid the pedestrians while following an acceptable trajectory.

11. CONCLUSION

The elastic band based connected collision avoidance method that uses V2P communication for avoiding car and pedestrian crashes was introduced in this paper. The paper concentrated on real-time implementation of the elastic band pedestrian collision avoidance method. Combined with V2P communication, this method is well suited for the situations where line-of-sight perception sensors fail due to a NLOS pedestrian presence. The effectiveness of this method was demonstrated using both HiL simulations and an experimental evaluation with our low speed autonomous shuttle. Interesting and relevant concepts like the effect of the digital divide on pedestrian safety as the smartphones that are needed for V2P communication may not be affordable in some parts of the world and whether or not authorities should ask pedestians to charge their mobile devices that will be used for V2P communication fully were not treated in this paper.

ACKNOWLEDGEMENT–This work was supported in part by the U.S. Department of Transportation Mobility 21: National University Transportation Center for Improving Mobility (CMU) sub-project titled: SmartShuttle: Model Based Design and Evaluation of Automated On-Demand Shuttles for Solving the First-Mile and Last-Mile Problem in a Smart City.

REFERENCES

Ararat, O. and Aksun-Guvenc, B. (2008). Development of a collision avoidance algorithm using elastic band theory. *IFAC Proc. Volumes* **41**, **2**, 8520–8525.

Avanish, H., Naik, B. A., Gaonkar, P. K. and Basavraj, A. (2013). Car to car communication for enhancing highway safety and cooperative collision avoidance. *Int. J. Engineering Research & Technology (IJERT)* **2**, **5**, 1614–1618.

Bagheri, M., Siekkinen, M. and Nurminen, J. K. (2016). Cloud-based pedestrian road-safety with situation-adaptive energy-efficient communication. *IEEE Intelligent Transportation Systems Magazine* **8**, **3**, 45–62.

Cho, W. (2014). Safety enhancement service for vulnerable users using P2V communications. *Proc. Int. Conf. Connected Vehicles and Expo*, Vienna, Austria.

David, K. and Flac, A. (2010). CAR-2-X and pedestrian safety. *IEEE Vehicular Technology Magazine* **5**, **1**, 70–76.

Elbatt, T., Goel, S. K., Holland, G., Krishnan, H. and Parikh, J. (2006). Cooperative collision warning using dedicated short range wireless communications. *Proc. 3rd Int. Workshop on Vehiclular Ad Hoc Networks*, Los Angeles, California.

Emirler, M., Wang, H. and Aksun-Guvenc, B. (2016). Socially acceptable collision avoidance system for vulnerable road users. *IFAC-PapersOnLine* **49**, **3**, 436–441.

Emirler, M., Wang, H., Aksun-Guvenc, B. and Guvenc, L. (2015). Automated robust path following control based on calculation of lateral deviation and yaw angle error. *Proc. ASME Dynamic Systems and Control Conf.*,

Columbus, Ohio, USA.
Gandhi, T. and Trivedi, M. M. (2007). Pedestrian protection systems: Issues, survey, and challenges. *IEEE Trans. Intelligent Transportation Systems* **8**, **3**, 413–430.
Gelbal, S., Aksun Guvenc, B. and Guvenc, L. (2017). SmartShuttle: A unified, scalable and replicable approach to connected and automated driving in a smart city. *Proc. 2nd Int. Workshop on Science of Smart City Operations and Platforms Engineering*, Pittsburg, Pennsylvania, USA.
Gomathi, C., Gandhimathi, D. and Dhivya, K. D. R. (2014). A review on vehicle-to-vehicle communication protocols for traffic safety using co-operative collision warning. *Int. J. Advance Research in Computer Science and Management Studies* **2**, **10**, 278–287.
Guvenc, L., Aksun-Guvenc, B., Demirel, B. and Emirler, M. T. (2017a). *Control of Mechatronic Systems*. IET. London, UK.
Guvenc, L., Aksun-Guvenc, B. and Emirler, M. (2017b). Connected and Autonomous Vehicles. *Internet of Things/Cyber-Physical Systems/Data Analytics Handbook*. Wiley. Hoboken, New Jersey, USA.
Hickey, K. (2016). NYC Looks to Tech to Improve Pedestrian Safety. https://gcn.com/articles/2016/10/19/nyc-ped-sig.aspx
Ho, P.-F. and Chen, J.-C. (2017). WiSafe: Wi-Fi pedestrian collision avoidance system. *IEEE Trans. Vehicular Technology* **66**, **6**, 4564–4578.
http://www.who.int/violence_injury_prevention/publications/road_traffic/decade_booklet/en
Intelligent Transportation Systems Joint Program Office-Office of the Assistant Secretary for Research and Technology (2016). DSRC: The Future of Safer Driving. http://www.its.dot.gov/factsheets/dsrc_factsheet.htm
Jiménez, F., Naranjo, J. E. and Gómez, Ó. (2015). Autonomous collision avoidance system based on accurate knowledge of the vehicle surroundings. *IET Intelligent Transport Systems* **9**, **1**, 105–117.
Kenney, J. B. (2011). Dedicated short-range communications (DSRC) standards in the United States. *Proc. IEEE* **99**, **7**, 162–1182.
Misener, J. A., Biswas, S. and Larson, G. (2011). Development of V-to-X systems in North America: The promise, the pitfalls and the prognosis. *Computer Networks* **55**, **14**, 3120–3133.
Paier, A., Faetani, D. and Mecklenbräuker, C. F. (2010). Performance evaluation of IEEE 802.11p physical layer infrastructure-to-vehicle real-world measurements. *Proc. 3rd Int. Symp. Applied Sciences in Biomedical and Communication Technologies*, Rome, Italy.
Quinlan, S. and Khatib, O. (1993). Elastic bands: Connecting path planning and control. *Proc. IEEE Int. Conf. Robotics and Automation*, Atlanta, Georgia, USA.
Sorokowska, A., Sorokowski, P., Hilpert, P. *et al*. (2017). Preferred interpersonal distances: A global comparison. *J. Cross-Cultural Psychology* **48**, **4**, 577–592.
Swanson, E., Yanagisawa, M., Najm, W. G., Foderaro, F. and Azeredo, P. (2016). Crash Avoidance Needs and Countermeasure Profiles for Safety Applications Based on Light-vehicle-to-pedestrian Communications. Washington, DC: National Highway Traffic Safety Administration (NTHSA).
Themann, P., Kotte, J., Raudszus, D. and Eckstein, L. (2015). Impact of positioning uncertainty of vulnerable road users on risk minimization in collision avoidance systems. *Proc. IEEE Intelligent Vehicles Symp.*, Seoul, Korea.
United States Department of Transportation (2017). United States Department of Transportation Intelligent Transportation Systems Joint Program Office-V2P Narration. https://www.its.dot.gov/communications/media/V2P_Narration.mp4
Verma, N., Kumar, G., Siddhant, A., Nama, P., Raj, A., and Mustafa, A. (2015). Vision based obstacle avoidance and recognition system. *Proc. IEEE Workshop on Computational Intelligence: Theories, Applications and Future Directions (WCI)*, Kanpur, India.
Wang, H., Tota, A., Aksun-Guvenc, B. and Guvenc, L. (2018). Real time implementation of socially acceptable collision avoidance of a low speed autonomous shuttle using the elastic band method. *IFAC Mechatronics J.*, **50**, 341–355.
Wang, L., Huang, W., Liu, X. and Tian, Y. (2012). Vehicle collision avoidance algorithm based on state estimation in the roundabout. *Proc. Int. Conf. Intelligent Control and Information Processing*, Dalian, China.
Wang, S.-Y., Cheng, Y.-W., Lin, C.-C., Hong, W.-J. and He, T.-W. (2008). A vehicle collision warning system employing vehicle-to-infrastructure communications. *Proc. IEEE Wireless Communications and Networking Conf.*, Las Vegas, Nevada, USA.
WHO (2011). Decade of Action for Road Safety 2011-2020: Saving Millions of Lives.